# Interpreting Optical Mapping Recordings in the Ischemic Heart: A Combined Experimental and Computational Investigation

Sara Dutta[1], Martin J. Bishop[1], Pras Pathmanathan[1], Peter Lee[2], Peter Kohl[2], T. Alexander Quinn[2], and Blanca Rodriguez[1]

[1] Computing Laboratory, University of Oxford, UK
[2] Harefield Heart Science Centre, Imperial College London, UK

**Abstract.** The occlusion of a coronary artery results in myocardial ischemia, significantly disturbing the heart's normal electrical behavior, with potentially lethal consequences, such as sustained arrhythmias. Biologists attempt to shed light on underlying mechanisms with optical voltage mapping, a widely used technique for non-contact visualization of surface electrical activity. However, this method suffers from signal distortion due to fluorescent photon scattering within the biological tissue. The distortion effect may be more pronounced during ischemia, when a gradient of electrophysiological properties exists at the surface of the heart due to diffusion with the surrounding environment. In this paper, a combined experimental and computer simulation investigation into how photon scattering, in the presence of ischemia-induced spatial heterogeneities, distorts optical mapping recordings is performed. Dual excitation wavelength optical mapping experiments are conducted in rabbit hearts. In order to interpret experimental results a computer simulation study is performed using a 3D model of ischemic rabbit cardiac tissue combined with a model of photon diffusion to simulate optical mapping recordings. Results show that the presence of a border zone, in combination with fluorescent photon scattering, distorts the optical signal. Furthermore, changes in the illumination wavelength can alter the relative contribution of the border zone to the emitted signal. The techniques developed in this study may help with interpretation of optical mapping data in electrophysiological investigations of myocardial ischemia.

## 1 Introduction

Sudden cardiac death accounts for over 300, 000 deaths in the US each year [1]. One of the major causes of cardiac arrest is coronary artery occlusion, reducing the supply of blood to the heart, and resulting in a phenomenon known as myocardial ischemia.

The ischemic action potential (AP) displays significant morphological changes: a decrease in upstroke velocity, AP amplitude and duration, and a depolarization of the resting membrane potential. These changes are mainly due to an increase in extracellular potassium concentration ($[K^+]_o$), a decrease in conductance of the main ion channels carrying sodium and calcium ($I_{Na}$ and $I_{CaL}$) and

D.N. Metaxas and L. Axel (Eds.): FIMH 2011, LNCS 6666, pp. 20–27, 2011.

an increase in conductance of the ATP-sensitive potassium current ($I_{K(ATP)}$) [2]. However, during ischemia, a layer of cells between poorly- and well-perfused tissue, referred to as the border zone (BZ), does not display fully ischemic action potentials (APs) [3,4], and the resulting electrophysiological heterogeneities increase the likelihood of developing disturbed excitation patterns and cardiac arrhythmias [5]. During global ischemia, this occurs at the the epi- and endocardial surface (with a BZ thickness of ≈1mm), due to diffusion of oxygen and ions with the environment surrounding the heart and blood within the ventricles [6].

Optical mapping utilizes voltage-sensitive fluorescent dyes to visualize the electrical activity of the heart. Upon excitation at a specific illumination wavelength, dye molecules transduce differences in membrane potential ($V_m$) into changes in emitted fluorescence. However, penetration of the illuminating light into the tissue (with depth dependent on illumination wavelength [7]) and scattering of the emitted fluorescent photons, means that the detected signal represents a weighted-average of $V_m$ levels from within a volume of tissue beneath the surface recording site. Such effects have been shown in modeling studies to distort optical recordings [8,9], in particular causing a prolongation of the AP upstroke.

In this study, we combine experiments and computational modeling to investigate how optical mapping recordings are affected by ischemia-induced transmural electrophysiological heterogeneity in the epicardial BZ and photon scattering. We hypothesize that optical signals will be significantly distorted relative to actual epicardial APs due to the collection of signals from a depth of tissue containing the BZ and fully ischemic myocardium. Preliminary dual-wavelength optical mapping experiments were performed on no-flow globally ischemic rabbit hearts. Two excitation wavelengths were used to investigate whether differences between the respective emitted optical signals would appear with time, assuming ischemia-induced transmural heterogeneities became more pronounced. Computational simulations, representing both the BZ and the effects of photon scattering on optical mapping signals, were performed to assist interpretation of experimental data.

## 2 Methods

### 2.1 Optical Mapping Experiments

Optical mapping experiments were performed on isolated rabbit hearts (1kg females, n=3), Langendorff-perfused with 37°C Krebs-Henseleit solution bubbled with 95% $O_2$ / 5% $CO_2$, and maintained in a heated imaging chamber filled with perfusate. Hearts were stained with voltage-sensitive dye (20$\mu$L bolus of 27.3mM di-4-ANBDQPQ), excitation-contraction uncoupled to eliminate motion-induced imaging artifacts (10$\mu$M blebbistatin), paced at the apex (2ms, 8V bipolar pulse at 1.25Hz, to ensure maintained capture and avoid alternans during ischemia), and subjected to no-flow global ischemia. Fluorescence was excited using camera frame-synchronized LED illumination, alternating $470 \pm 10$nm (shallow penetration) and $640 \pm 10$nm (deep penetration), and acquired with a 690nm long-pass filter (which effectively cuts out excitation light) at 922Hz (64x64 pixel 16-bit

CCD camera resulting in 300$\mu$m/pixel resolution). This allowed paired comparison of short and long wavelength excitation.

### 2.2 Modeling Ischemia-Induced Alterations in Electrophysiology

We constructed a cuboid ventricular segment model (5mm x 5mm x 5mm) of global ischemia, including transmurally-rotating fiber architecture and rabbit ventricular cell membrane dynamics [10], with an added $I_{K(ATP)}$ current [11]. We chose to model the cardiac tissue after 10min of ischemia, as the electrophysiological differences between the healthy and ischemic tissue are assumed to be greatest at that time [6]. The BZ, as shown in Figure 1, was represented by a transmural gradient in ischemia-induced changes [6].

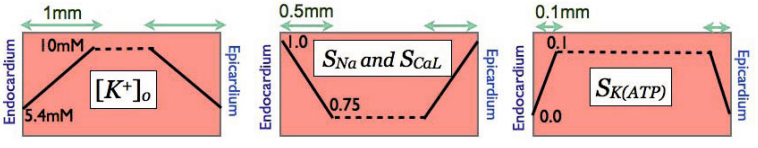


**Fig. 1.** Diagram of varying ischemic electrophysiological parameters of the cardiac tissue model with a BZ: $[K^+]_o$, $S_{Na}$, $S_{CaL}$, and $S_{K(ATP)}$ define a BZ of 1mm, 0.5mm, and 0.1mm, respectively

Bidomain simulations, solved using the finite element method within the Chaste environment [12], were used to simulate propagation of electrical excitation through the tissue following a supra-threshold stimulus applied to the bottom plane of the cube, horizontally aligned to the transmural section. To assess the effects of the BZ, models with/without ischemia-induced spatial heterogeneities were considered.

### 2.3 Optical Mapping Model

Optical mapping signals were simulated using the model presented by Bishop *et al.* [8]. Briefly, the steady-state photon diffusion equation was solved using the finite element method in the Chaste environment to calculate the distribution of photon density throughout the tissue following both uniform epicardial illumination ($\Phi_{illum}$) and the resulting fluorescent photon emission ($\Phi_{em}$): $D \bigtriangledown^2 \Phi - \mu_a \Phi = -w$, where the optical diffusivity ($D$) and absorptivity ($\mu_a$) were taken at the illumination/emission wavelength (488/669nm): 0.18/0.36mm, 0.52/0.10mm$^{-1}$ [8]. Zero boundary conditions were used throughout, except during illumination where the source term $w$ was set to an arbitrary value of 1 on the epicardial surface; during emission, $w$ was defined to be a function of $\Phi_{illum}$ and $V_m$, as obtained from the bidomain simulations, at each point in the tissue. The recorded optical signal, $V_{opt}$, was then calculated as the outward flux of $\Phi_{em}$ at each time step across the epicardial surface by applying Fick's Law: $V_{opt} = -D^{em} \bigtriangledown \Phi_{em}.\boldsymbol{n}$, where $\boldsymbol{n}$ is the normal to the epicardial surface.

The degree of distortion due to photon scattering depends highly on the effective optical penetration depth ($\delta = \sqrt{D/\mu_a}$) at both the illumination and emission wavelengths [8]. Therefore, we analyzed the effects of high/default/low values of $\delta_{eff}^{illum}$ (2.45/0.59/0.18mm) and $\delta_{eff}^{em}$ (3.20/1.90/0.18mm) to represent high and low wavelength penetration depths.

### 2.4 Data Analysis

The results presented are taken from normalized $V_m$ and $V_{opt}$ values of a node at the center of the epicardium: $V_m^*$ and $V_{opt}^*$. We calculate the APD as the time difference between the upstroke reaching 0 mV and 90% repolarization and upstroke duration as the time between $V_m$ reaching 10% and 90% depolarization. We define $\tau_{opt}$ as the ratio of $V_{opt}^*$ and $V_m^*$.

## 3 Results

### 3.1 Optical Mapping Experiments

Experiments were performed in isolated rabbit hearts to investigate changes in optical mapping signals during no-flow global ischemia. Normalized voltage signals, showing the activation wavefront at different times following apical stimulation can be seen in Figure 2(a). Upstrokes from a 2x2 pixel area on the left ventricular free wall for the two excitation wavelengths at different times of ischemia are shown in Figure 2(b). Differences between the respective emitted optical signals increase with time, showing a prolongation in upstroke duration and a reduced upstroke velocity recorded with 640nm compared to 470nm excitation. We hypothesize that the deeper penetrating wavelength (640nm) displays more ischemic features, as it gathers information from a larger volume that includes more ischemic cells than the shallower penetrating wavelength (470nm). To investigate the source of these differences, we subsequently performed a simulation study.

### 3.2 Border Zone Effects on Epicardial Transmembrane Potential

Figure 3(a) shows the distribution of $V_m^*$ for the two types of tissue: with and without a BZ. We notice that the repolarization wavefront shapes are significantly different in the two types of tissue. Cells close to the epicardium and endocardium depolarize faster and take longer to repolarize in the tissue with a BZ, than in the homogeneously ischemic tissue.

Figure 3(b) shows that the AP (sampled from the epicardium) of the fully ischemic tissue (without a BZ) displays all of the expected ischemia-induced morphological changes. In the presence of a BZ, the AP displays an upstroke duration 22% shorter and an APD 11% longer than the homogeneously ischemic tissue, characteristics of an AP from less ischemic tissue.

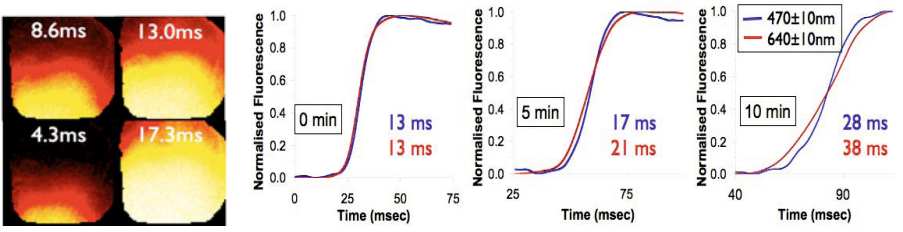


(a) (b)

**Fig. 2.** (a) Images of normalized fluorescence emitted from the left ventricle of the rabbit heart at different times after apical stimulation. (b) Normalized voltage upstroke after 0, 5 and 10 min of ischemia for 470nm ±10nm and 640 ±10nm excitation with the respective upstroke durations.

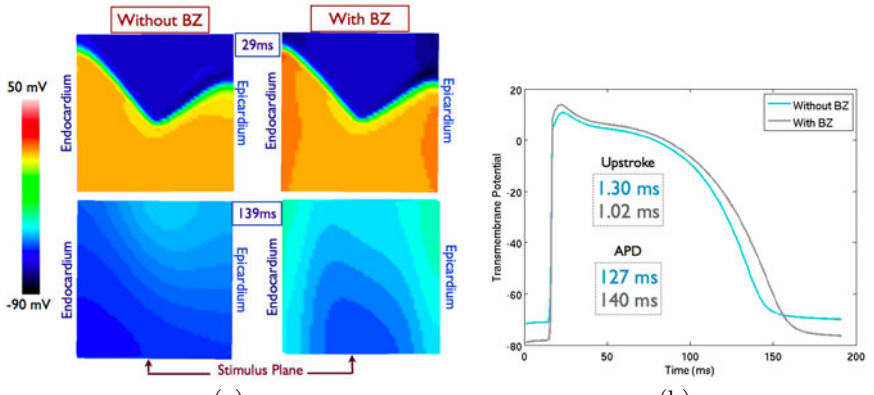


(a) (b)

**Fig. 3.** Computational model of border zone effects on $V_m^*$. (a) Snapshots of $V_m^*$ for tissue with and without a BZ during tissue depolarization (29 ms) and repolarization (139 ms) following apical stimulation (b) $V_m^*$ with and without a BZ, including APD and upstroke duration values.

### 3.3 Optical Signal and Transmembrane Potential Comparison

Figure 4(a) shows the corresponding $V_{opt}^*$ surface optical APs with/without BZ, whilst Figure 4(b) compares differences in upstroke duration and APD relative to the $V_m^*$ traces of Figure 3(b). As has been shown in previous optical mapping studies, the emitted signal represents the transmembrane potential of a weighted average volume of myocardium, due to photon scattering [8,9]. These effects are more noticeable in the upstroke than the APD, as shown in Figure 4(b), even in the homogeneously ischemic tissue. This is caused by the narrow and fast wavefront that occurs during depolarization, such that as it crosses the scattering

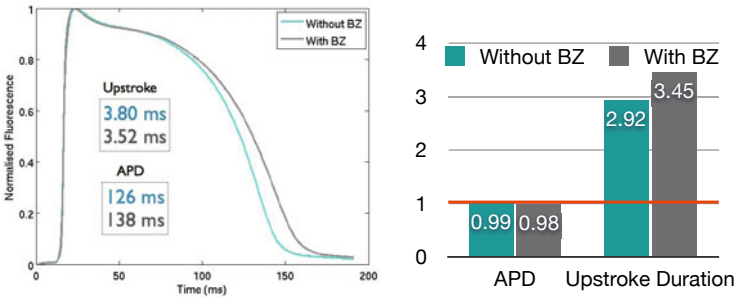


(a) (b)

**Fig. 4.** (a) Simulated $V^*_{opt}$ with and without BZ. APD and upstroke duration values are shown for the respective APs. (b) Photon scattering effects, represented by $\tau_{opt}$, on APD and upstroke duration for simulations run on a tissue with and without a BZ.

volume, some cells are in their resting state while others are excited. This is not the case during the slower repolarization phase, where most of the cells in the scattering volume will have a similar transmembrane potential. In fact, $\tau_{opt(APD)}$ values are close to 1 while $\tau_{opt(upstroke)}$ values are of 2.92 or greater. Therefore, differences in APD seen in Figure 4(a) are mainly due to the border zone as opposed to photon scattering.

Figure 4(b) shows that $\tau_{opt}$ values move away from 1 in the presence of a BZ for both APD and upstroke duration. This arises from the increase in heterogeneities which lead to differences in AP morphology, in conduction velocity and wave front propagation. In the presence of a BZ, $V^*_{opt}$ gathers information from cells exposed to different degrees of ischemia, while $V^*_m$ represents the less ischemic cells at the epicardium. Differences in upstroke duration and APD for simulations with and without a BZ are attenuated in $V^*_{opt}$ (Figure 4(a)) compared to $V^*_m$ (Figure 3(b)) due to the optical signal representing a weighted average volume of tissue.

### 3.4 Varying Optical Mapping Penetration Depth

The trends mentioned above are accentuated as we change the penetration depth. Figure 5 shows that $\tau_{opt}$ values move away from 1 as the penetration depth increases for both APD and upstroke duration in simulations with and without a BZ. Differences between $V^*_{opt}$ and $V^*_m$ increase due to the optical signal averaging over a bigger volume for an increased penetration depth. Furthermore, the differences between $\tau_{opt}$ values with and without a BZ become more pronounced for both upstroke duration and APD calculations as the penetration depth increases. As we increase $\delta_{eff}$, the differences between $V^*_{opt}$ with and without a border zone are attenuated due to a larger scattering volume, such that more signal is acquired from the deeper ischemic tissue, decreasing the relative

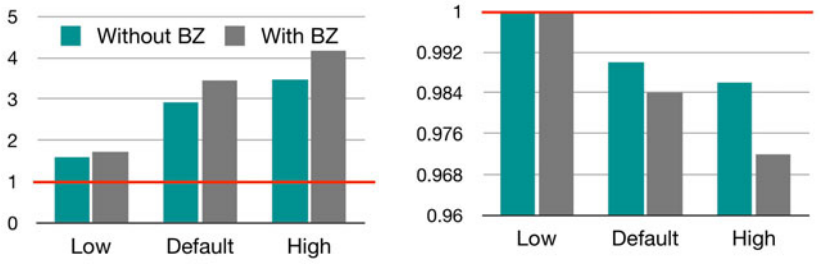


**Fig. 5.** Varying penetration depth effects, represented by $\tau_{opt}$, for tissue with and without a BZ. (a) Upstroke duration and (b) APD, taken at different penetration depths (Low, Default, and High).

contribution of the BZ. However, a large change remains in $V_m^*$ with/without BZ (Figure 3(b)), thus leading to a larger difference in $\tau_{opt}$ as penetration depth increases.

## 4 Conclusions

The aim of this study was to investigate the combined effects of ischemia-induced transmural heterogeneities and photon scattering on epicardial optical mapping recordings in a globally ischemic heart. We approached this with a combined experimental and simulation study. Preliminary dual wavelength optical mapping experiments in globally ischemic isolated hearts were performed. These showed a clear difference in voltage-sensitive fluorescence emission between the two excitation wavelengths, which we attribute to the presence of an epicardial BZ. We investigated this hypothesis with a model of global ischemia, including transmural variation of electrophysiological parameters, combined with a model of photon density and excitation to simulate the optical signal at the surface of the heart. Simulations of $V_m$ and $V_{opt}$ were conducted on a model of ischemic rabbit tissue with and without a BZ. This demonstrated that the electrophysiological heterogeneities that exist in the presence of an epicardial BZ affect the optical signal, resulting in a decrease in upstroke duration and an increase in APD compared to the optical signal from a homogeneously ischemic slab of tissue. Furthermore, as the penetration depth of the optical signal is increased, the differences between the epicardial $V_{opt}$ and $V_m$ are accentuated.

Overall, this study shows that the electrophysiological heterogeneities that arise at the epicardial surface during ischemia have a significant effect on optical mapping recordings. Furthermore, exciting fluorescent dyes with different wavelengths has an important impact on the resulting optical signal and may be used to investigate transmural heterogeneities. These findings provide new insights into optical mapping data interpretation when investigating the role of heterogeneity during global ischemia.

## References


1. Papadakis, M., Sharma, S., Sheppard, M., Panoulas, V., Behr, E.: The magnitude of sudden cardiac death in the young: a death certificate-based review in England and Wales. Europace 11, 1353–1358 (2009)
2. Carmeliet, E.: Cardiac ionic currents and acute ischemia: from channels to arrhythmias. Physiol. Rev. 79, 917–987 (1999)
3. Fiolet, J., Baartscheer, A., Schumacher, C., Terwelle, H., Krieger, W.: Transmural inhomogeneity of energy metabolism during acute global ischemia in the isolated rat heart: dependence on environmental conditions. J. Mol. Cell. Cardiol. 17, 87–92 (1985)
4. Schaapherder, A., Schumacher, A., Coronel, R., Fiolet, J.: Transmural inhomogeneity of extracellular [K+] and pH and myocardial energy metabolism in the isolated rat heart during acute global ischemia; dependence on gaseous environment. Basic Res. Cardiol. 85, 33–44 (1990)
5. Rodriguez, B., Trayanova, N., Noble, D.: Modeling cardiac ischemia. Ann. NY Acad. Sci. 1080, 395–414 (2006)
6. Tice, B., Rodriguez, B., Eason, J., Trayanova, N.: Mechanistic investigation into the arrhythmogenic role of transmural heterogeneities in regional ischemia phase 1A. Europace 9, 47–58 (2007)
7. Walton, R., Benoist, D., Hyatt, C., Gilbert, S., White, E., Bernus, O.: Dual excitation wavelength epifluorescence imaging of transmural electrophysiological properties in intact hearts. Heart Rhythm 7, 1843–1849 (2010)
8. Bishop, M., Rodriguez, B., Eason, J., Whiteley, J., Trayanova, N., Gavaghan, D.: Synthesis of voltage-sensitive optical signals: application to panoramic optical mapping. Biophys. J. 90, 2938–2945 (2006)
9. Hyatt, C., Mironov, S., Wellner, M., Berenfeld, O., Popp, A., Weitz, D., Jalife, J., Pertsov, A.: Synthesis of voltage-sensitive fluorescence signals from three-dimensional myocardial activation patterns. Biophys. J. 85, 2673–2683 (2003)
10. Mahajan, A., Shiferaw, Y., Sato, D., Baher, A., Olcese, R., Xie, L., Yang, M., Chen, P., Restrepo, J., Karma, A., Garfinkel, A., Qu, Z., Weiss, J.: A rabbit ventricular action potential model replicating cardiac dynamics at rapid heart rates. Biophys. J. 94, 392–410 (2008)
11. Michailova, A., Suacerman, J., Belik, M., McCulloch, A.: Modeling regulation of cardiac KATP and L-type Ca2+ currents by ATP, ADP, and Mg2+. Biophys. J. 88, 2234–2249 (2005)
12. Pitt-Francis, J., Pathmanathan, P., Bernabeu, M., Bordas, R., Cooper, J., Fletcher, A., Mirams, G., Murray, P., Osborne, J., Walter, A., Chapman, S., Garny, A., van Leeuwen, I., Maini, P., Rodriguez, B., Waters, S., Whiteley, J., Byrne, H., Gavaghan, D.: Chaste: A test-driven approach to software development for biological modelling. Comput. Phys. Commun. 180, 2452–2471 (2009)